Optical properties of $Cu_2ZnSn(S_xSe_{1-x})_4$ solar absorbers: Spectroscopic ellipsometry and *ab initio* calculations

Shu-yi Li,[1,a)] Sergiy Zamulko,[2] Clas Persson,[2,3] Nils Ross,[1,2] Jes K. Larsen,[1] and Charlotte Platzer-Björkman[1,b)]
[1]*Ångström Solar Center, Solid State Electronics, Uppsala University, Uppsala SE-75121, Sweden*
[2]*Department of Physics/Centre for Materials Science and Nanotechnology, University of Oslo, Oslo NO-0316, Norway*
[3]*Department of Materials Science and Engineering, Royal Institute of Technology, Stockholm SE-10044, Sweden*

(Received 26 October 2016; accepted 14 December 2016; published online 11 January 2017)

Dielectric functions of $Cu_2ZnSn(S_xSe_{1-x})_4$ thin film absorbers with varied x were determined by spectroscopic ellipsometry and *ab initio* calculations. From the combination of experimental and theoretical studies, the fundamental interband transition energy E_0 (~1–1.5 eV) and the next following transition energy E_1 (~2–3 eV) were identified and found to blue-shift with increasing sulfur anion content, while keeping the energy separation E_1-E_0 almost constant, ~1.4 eV from experiments, and 1 eV from theory. In addition, the average dielectric responses were found to decrease with sulfur anion content from both theoretical and experimental results. The Tauc optical bandgap value E_g determined on samples prepared on Mo and soda lime glass substrate showed a positive linear relationship between x and bandgap E_g. The bandgap bowing factor determined from the theoretical data is 0.09 eV. [http://dx.doi.org/10.1063/1.4973353]

Possessing the advantage of earth abundancy and a favorable size of bandgap, compounds based on kesterite $Cu_2ZnSn(S_xSe_{1-x})_4$ have attracted great attentions for applications as thin film solar cells. Since the first kesterite solar cell with 0.66% solar conversion efficiency,[1] decades of research have led to substantial improvements with current record efficiencies 9.2% for pure sulfides and 12.6% for $Cu_2ZnSn(S_xSe_{1-x})_4$ (CZTSSe).[2] Approaches involving bandgap grading by partial anion substitution of S with Se and/or cation substitution of, for example, Sn with Ge are considered to be the promising and logical next step.[3–6] For this purpose, fundamental properties such as dielectric functions for kesterite $Cu_2ZnSn(S_xSe_{1-x})_4$ are the essential inputs to explore the effect of various device designs and the interface properties through device modeling. Device modeling is, in many cases, the only practical approach to separate optical and electrical losses and understand the effect of bandgap grading towards front and back interfaces, and thereby provide us the key knowledge to separate the interface recombination and the bulk recombination due to strong band tailing, which is a prerequisite for understanding limitations of CZTSSe devices. The experimental data in literature so far have been focused on the cases for $x = 0$ and 1.[7–11] This work presents the dielectric functions of CZTSSe in the intermediate region $0 \le x \le 1$ with data collected from ellipsometry measurements as well as *ab initio* calculations.

$Cu_2ZnSn(S_xSe_{1-x})_4$ (CZTSSe) absorbers were deposited on bare and Mo-coated soda lime glass substrates (SLG) by magnetron co-sputtering from CuS, ZnS, and SnS compound targets in an argon atmosphere and followed by a rapid annealing process in a selenium atmosphere.[12] The selenizations were done in the same fashion as by Larsen *et al.*[13] In order to achieve different anion ratios in the samples, the selenization temperature and duration were set for S1(S1′), S2(S2′), and S3(S3′) in Table I as 530 °C 10 min, 560 °C 4 min, and 500 °C, 10 min, respectively. The pure sulfide sample referred to as S4 in Table I was taken from our pervious work.[9] Metallic elemental ratios Cu/Zn and Cu/(Zn+Sn) were determined by X-ray fluorescence (XRF, PANalytical Epsilon 5) to be 1.81 and 0.92 for S1–S3 on Mo/SLG and S1′–S3′ on SLG. That of S4 was 1.39, 0.80. X-ray photoelectron spectroscopy (XPS, Quantum 2000 scanning ESCA Microscope) depth profiling were conducted under Al kα illumination with argon ion gun at 0.5 keV for sputtering, and the results (not shown) confirmed homogeneous depth distribution of the elements in the samples. By means of X-ray diffraction (XRD, Siemens D 5000 diffractometer, CuKα irradiation) and Raman spectroscopy (Renishaw inVia system, 532 nm laser excitation), the samples were confirmed to be kesterite CZTSSe (see "supplementary material" for details). The anion ratios $x = S/(S+Se)$ were determined by XRD to be 0.23, 0.27, and 0.38 for S1–S3 produced on Mo/SLG, and 0.24, 0.29, and 0.46 for corresponding samples S1′–S3′ on SLG substrates as shown in Table I (more details in "supplementary material"). It is worth noticing that the selenization seems more prevalent on samples deposited on the Mo-coated glass than the bare ones. Although SnSe and ZnSe were not detected with XRD or Raman, a small amount (around 2 vol. % from XRF composition assuming standard unit cell volumes) of these secondary phases are estimated to

a)shuyi.at.uu@gmail.com
b)Author to whom correspondence should be addressed. Electronic mail: Charlotte.Platzer@angstrom.uu.se

TABLE I. Compositional, optical, and theoretical data for $Cu_2ZnSn(S_xSe_{1-x})_4$ absorber films. S1–S3 are the samples produced on Mo/SLG with S1′–S3′ as their counterparts on SLG. The theoretical results derived from *ab initio* calculations for $x = 0$, 0.25, 0.5, 0.75, and 1 are also shown for both HSE06, $mBJ + U_d$ and $mBJ + U_d + \Delta_g$ methods.

Samples or *ab initio* calc	x	$E_{g,Tauc}$ or $E_{g,calc}$ (eV)	E_0 (eV)	E_1 (eV)	ε_0	ε_∞
S1/S1′	0.23/0.24	1.16/1.19	1.15	2.54	…	…
S2/S2′	0.27/0.29	1.18/1.2	1.16	2.55	…	…
S3/S3′	0.38/0.46	1.24/1.27	1.23	2.62	…	…
S4	1	1.55	1.6	3.09	…	…
HSE06	0	0.73	0.76	2.30	11.2	8.7
$mBJ + U_d$		0.83	0.81	1.75	10.9	8.4
$mBJ + U_d + \Delta_g$		1.08	1.01	2.00	10.4	7.9
HSE06	0.25	0.85	0.88	2.38	10.1	8.2
$mBJ + U_d$		0.91	0.86	1.83	10.0	8.0
$mBJ + U_d + \Delta_g$		1.16	1.10	2.09	9.5	7.5
HSE06	0.5	0.99	1.06	2.50	9.8	7.7
$mBJ + U_d$		0.99	0.95	1.91	9.8	7.6
$mBJ + U_d + \Delta_g$		1.24	1.20	2.17	9.4	7.2
HSE06	0.75	1.10	1.19	2.61	9.6	7.3
$mBJ + U_d$		1.07	1.05	1.99	9.6	7.2
$mBJ + U_d + \Delta_g$		1.32	1.28	2.26	9.2	6.8
HSE06	1	1.26	1.30	2.71	9.3	6.7
$mBJ + U_d$		1.19	1.15	2.09	9.3	6.8
$mBJ + U_d + \Delta_g$		1.44	1.36	2.35	9.0	6.5

be present but not enough to significantly impact the optical properties from the view point of effective medium theories.[14,15]

For surface roughness reduction, samples were polished using colloidal silica suspension (OP-S, 0.04 μm, Struers). The scanning electron microscopy (SEM, Zeiss Merlin field emission microscope) images of S1 before and after polishing shown in Figs. 1(a) and 1(b) demonstrate that significant amount of surface roughness was removed by the polishing process. However, some of the deep grooves in between grains in Fig. 1(b) remain in the otherwise very flat surface. Also shown is a surface image of unpolished S1′ on SLG in Fig. 1(c), with much smaller grains compared to unpolished S1 on Mo. This tendency was seen when comparing all the corresponding sample pairs (i.e., S# and S#′) and can be correlated to the lower Se content in samples fabricated on the SLG substrate indicated by XRD results. The SEM cross section image (not shown) also showed a thick layer of $MoSe_x$ for all the samples. Atomic force microscopy (AFM, PISA XE-150) revealed that the root mean square (RMS) roughness were significantly reduced by polishing from originally 77–164 nm for CZTSSe samples to effectively 8–15 nm on the dominating flat part of surface without trails (16–36 nm including the trails), sufficiently smooth to be analyzed by means of spectroscopic ellipsometry without the need of an overly complex structure model.[9,16]

The spectroscopic ellipsometry (SE) measurements were carried out directly after polishing using a variable-angle spectroscopic ellipsometer (VASE) with a rotating analyzer and an enabled AutoRetarder (J.A.Woollam Co, Inc.). The ellipsometric functions Ψ and Δ were recorded at 65°, 70°, and 75° incidence angles in the wavelength range of 300–1700 nm. A multi-stack thin film model consisting of surface roughness layer (SRL)/CZTSSe/$MoSe_x$ (or MoS_x for S4)/Mo were used to describe the structure of samples S1–S4, and SRL/CZTSSe/SLG for S1′–S3′. The complex dielectric functions ε ($\varepsilon = \varepsilon_1 + i\varepsilon_2$) of CZTSSe were modeled with oscillator models[17] and the SRL was represented by Bruggeman effective medium theory[14] considering a mixture of CZTSSe and voids. Prior to the SE data analysis, the dielectric functions of $MoSe_x$ and Mo were determined by SE and the initial input of thicknesses of each layers were determined by SEM cross section imaging with complementary information gained from XRF measurements. The SE analysis were carried out by fitting the calculated Ψ and Δ derived from the optical model to the experimental data.

In parallel, the *ab initio* calculations were conducted by the projector augmented wave (PAW) method as implemented in the Vienna *ab initio* simulation package (VASP).[18] The bandgap energies and dielectric functions were calculated with Heyd-Scuseria-Ernzerhof hybrid functional with the standard screening parameter of 0.2 (HSE06).[19] We also

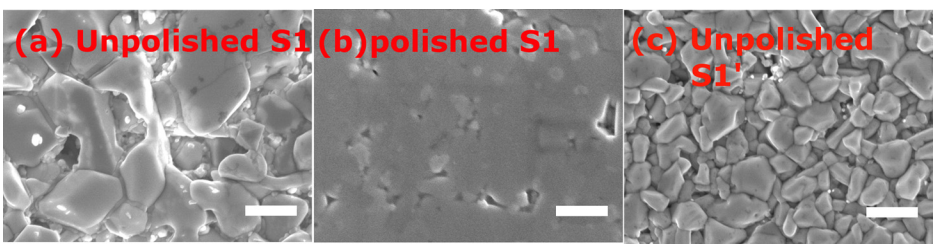

FIG. 1. SEM surface image of S1 before (a), after polishing (b), as well as S1′ before polishing (c).

employ the modified Becke-Johnson (mBJ) exchange-correlation functional[20] in conjunction with *ab initio*-derived U_d parameters,[21] (mBJ + U_d), with $U_d = 4.0$ eV and 7.5 eV for Cu-3*d*, Zn-3*d*, respectively. Here, U_d is an on-site Coulomb potential to correct the localization of *d*-like states. The PBEsol functional[22] was used for relaxation, which reproduces rather accurately the lattice constants of CZTS-type materials,[23] which is important for describing the crystalline structure. The calculations were performed for $Cu_2ZnSn(S_xSe_{1-x})_4$ alloys with $x = 0$, 0.25, 0.5, 0.75, and 1 in eight-atom primitive cells which thus involves periodicity of the anion lattices. We justify the small cells with a more accurate calculation of the optical properties regarding band dispersion and the **k**-space integration. The plane wave energy cutoff was 450 eV. In the relaxation process, the integration over the irreducible Brillouin zone was done with $10 \times 10 \times 10$ Γ-centered Monkhorst-Pack-like **k**-mesh. The HSE06 and mBJ + U_d calculations were performed with $6 \times 6 \times 6$ and $20 \times 20 \times 20$ **k**-meshes, respectively. The convergence tolerance for the total energy was 10^{-8} eV/atom and $5 \cdot 10^{-3}$ eV/Å for the forces on the atoms, considering full lattice and atom relaxations.

The results of experimentally ("exp") determined dielectric functions are shown in Fig. 2(a). The imaginary part ε_2 showed abrupt onsets at fundamental gap energies ~1–1.5 eV corresponding to E_0 CP energy for transitions between valence band maximum (VBM) and conduction band minimum (CBM) at Γ point (fundamental gap), and a shoulder at energy ~2.6–3 eV corresponding to E_1 CP energy for transitions in regions away from Γ point, where VBM and CBM exhibit flat features. Quantitative values of E_0 and E_1 can be extracted by CP analysis, which assumes analytical line shapes of ε as a function of photon energy $h\nu$

$$\varepsilon(h\nu) = C - Ae^{i\phi}(h\nu - E + i\Gamma)^m, \tag{1}$$

where the amplitude parameter *A*, CP energy threshold *E*, broadening Γ, excitonic phase angle ϕ, and exponent *m* can be determined by fitting second derivative of experimentally determined complex dielectric functions with analytical form of $d^2\varepsilon/d(h\nu)^2$

$$\frac{d^2\varepsilon}{d(h\upsilon)^2} = \begin{cases} -m(m-1)Ae^{i\phi}(h\upsilon - E + i\Gamma)^{m-2}, & m \neq 0, \\ Ae^{i\phi}(h\upsilon - E + i\Gamma)^{-2}, & m = 0. \end{cases} \tag{2}$$

In CP analysis,[24] exponent $m = 1/2$, 0 [logarithmic, $\ln(h\nu - E + i\Gamma)$], $-1/2$, and -1 correspond to 3D, 2D, 1D CPs, and discrete excitons, respectively. The dimensional assignments are related to details in joint density of states and band structure;[25] however, previous CP studies did not always agree regarding such assignments.[6–8,26,27] In this work, the purpose of CP analysis was to pin-point the threshold energy in a systematic and reproducible way; therefore, excitonic line shape was chosen since it gave the best fit at E_0 and E_1 for all samples. An example fit is shown in Fig. 2(c) for S1. The obtained threshold energies E_0 and E_1 are shown in Table I. It is clear that both E_0 and E_1 blue-shift as sulfur content increases but the separation between E_0 and E_1 remains the same, ~1.4 eV. The $E_1 - E_0$ difference is related to the generation profile of the device via absorption coefficient but its impact on the device performance is unlikely to be significant compared to other issues that CZTSSe typically suffer from, such as tail states.

The theoretically determined gap energies $E_{g,calc}$ calculated with HSE06 and mBJ + U_d functionals are qualitatively similar and agree well with earlier published theoretical data.[28–30] However, mBJ + U_d seems to underestimate the gap energies when compared with the experimental values, and we therefore corrected the gap by $\Delta_g = 0.25$ eV. The calculated dielectric functions obtained with the mBJ + U_d + Δ_g method [Fig. 2(b)] agree fairly well with the experimental results [Fig. 2(a)], showing the trend of increasing values of E_0 and E_1 CP peak positions with S content (0.35 eV from x = 0 to 1) as well as the constant energy differences between E_0 and E_1 peaks, ~1 eV for all anion compositions. However, the CPs from the mBJ + U_d + Δ_g method are, as expected,

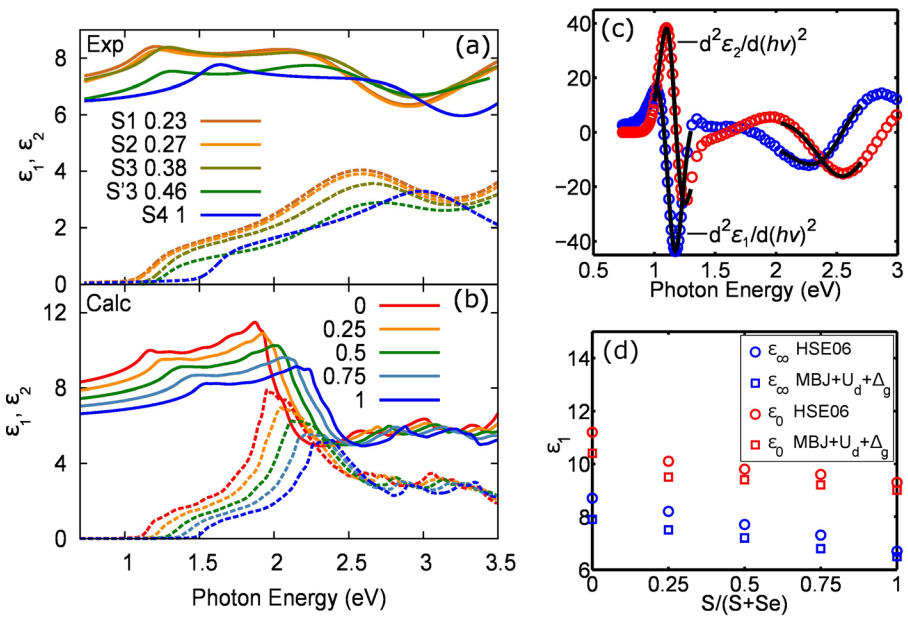

FIG. 2. ε_1 (solid line) and ε_2 (dashed line) determined by ellipsometry (a) and *ab initio* calculation (b), fit to $d^2\varepsilon/d(h\nu)^2$ from critical point analysis for S1 (c), and the theory-derived ε_∞, ε_0 as a function of S = S/(S + Se) (d).

somewhat too low in energy compared with the corresponding HSE06 values. From calculations of the electronic band structure (not shown; see Ref. 8) we find that the pronounced E_1 CP originates from transitions from the uppermost valence band to the lowest conduction band and around the P ($^1/_2$, $^1/_2$, $^1/_2$) point of the Brillouin zone (in the conventional coordinates).

Additionally, transitions from the four uppermost valence bands to the lowest conduction band at the Z (0,0,1) and Y_1 ($^1/_2$, $^1/_2$, -1) points also contribute to the E_1 CP. These transitions are at slightly higher ($\sim$0.1 eV) energies than at the P point. The experimental data exhibited much broader peaks likely due to carrier scattering[7,31] caused by polycrystallinity of the films.

The average dielectric functions for static and high frequency cases ε_0 and ε_∞ were determined with the HSE06 and mBJ+U_d functionals as well as with the corrected mBJ + U_d + Δ_g approach [Fig. 2(d)]. Values from the HSE06 calculations were slightly larger than for the corresponding mBJ+U_d; however, for $x = 1$ the value of dielectric constants are fairly equal for the three approaches. The difference between the static- and high-frequency constants is $\varepsilon_0 - \varepsilon_\infty \approx 3$, which indicates similar ionicity as for ZnS and ZnSe.[32] The calculated dielectric constants decrease with S substitution. This indicated the inverse relation between the trend of energy gap and the dielectric response qualitatively falls in line with the empirical relationship: (commonly known as Moss-Ravindra relations[33]) small bandgap implies large dielectric constant. However, the differences in the dielectric constants of the considered alloys are relatively small. The experimental data showed the same trend but with some degree of scattering due to the differences in grain structures and the challenge to produce samples with same grain structures but varied x. The large number of samples allowed us to compare those with similar grain structures and same substrates, e.g., S3 and S4. It can be clearly seen that both ε_1 and ε_2 are lowered when x changed from 0.38 to 1, which confirmed the trend predicted by theory.

The absorption coefficients of for S1–S3 are determined from SE data by $\alpha = (4\pi/\lambda)[(|\varepsilon| - \varepsilon_1)/2]^{1/2}$; those of S1′–S3′ were obtained from spectral transmission (T) and reflection (R) recorded in Perkin-Elmer Lambda 900 spectrophotometer and utilizing formula[34] $\alpha = (1/d)\ln[(1-R)/T]$ for a sample with thickness d. The Tauc optical gaps $E_{g,Tauc}$ were determined by "Tauc plot," which was originally intended for amorphous materials but also proven to generally give robust and accurate evaluations for materials of polycrystalline nature.[35] In the case of CZTSSe with direct bandgap, it was done by linearly extrapolating $(\alpha h\nu)^2$ vs $h\nu$ plot at the band edge as shown in Fig. 3. The resulting bandgap values were plotted as a function of $x = S/(S+Se)$ in the inset of Fig. 3. Spectrophotometry-determined α from S1′–S3′ was nearly identical to the optical properties determined by SE (not shown) in the transparent region of the films. Since the selenization was much less prevalent on the SLG substrate in this work, S1′–S3′ were not identical to S1–S3 in terms of x as originally intended, so they are used as extra data points in addition to S1–S3. Also shown in blue squares are the bandgap values from our previous work done

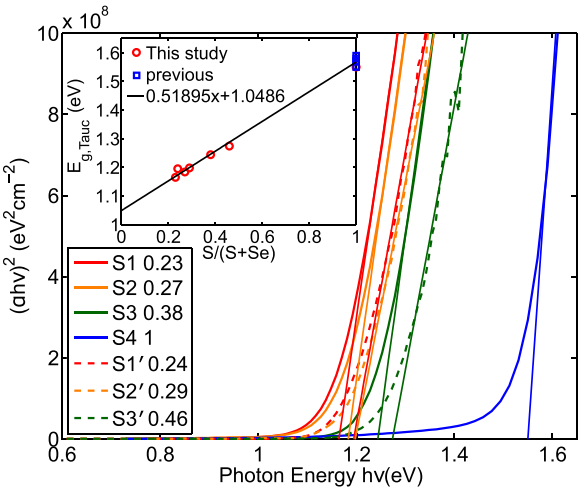

FIG. 3. Tauc plot $(\alpha h\nu)^2$ v.s. $h\nu$ from SE data for S1–4 and spectrophotometry data for S1′–S3′ and the resulting Tauc bandgap as a function of x = S/(S + Se) in the inset.

on CZTS.[9] The determined Tauc gaps $E_{g,Tauc}$ showed an linearly increasing trend with increasing x [Fig. 3, inset] in accordance with the current theoretically determined E_g and our findings regarding the CP energies [Table I] as well as with previous studies.[36,37] The bandgap energy bowing factor determined by the theoretical part of the current study is 0.09 eV, which falls in the same value range with those from previous theoretical studies[37] with 0.07 eV (HSE06), $\sim$0.1 eV (generalized gradient approximation), and 0.08 eV from optical absorption study.[36] We refrained from the experimental determination of the bowing factor judging from the limited distribution of data points.

In conclusion, the comprehensive study on the optical properties of kesterite $Cu_2ZnSn(S_xSe_{1-x})_4$ with intermediate sulfur content were conducted by combining both experimental (spectroscopic ellipsometry on CZTSSe absorbers) and theoretical (*ab initio* calculations) methods and the dielectric functions, bandgaps E_g and CP transition energies E_0, E_1 were determined. It was found that with increasing sulfur anion content x, E_g, E_0, and E_1 increased monotonically while E_0 and E_1 kept equal energy spacing, i.e., 1.4 eV from experimental and 1 eV from theoretical studies. In contrast, the dielectric responses ε_0 and ε_∞ were found to decrease with increasing x. The Tauc bandgap $E_{g,Tauc}$ was obtained from the experimental data and found to increase linearly from 1.16 eV to 1.55 eV with x increasing from 0.23 to 1. The bandgap bowing factor was determined to be 0.09 eV by the theoretical study. These results help clarifying the optical properties of kesterite $Cu_2ZnSn(S_xSe_{1-x})_4$ with $0 \le x \le 1$ and contribute essential fundamental knowledge for further studies such as device modeling.

See supplementary material for details regarding structure and phase analysis by x-ray diffraction and Raman scattering and dielectric functions of the $MoSe_x$ layer.

S.Y.L. would like to thank Erik Särhammer, Tove Ericson, Katharina Rudisch, Yi Ren for assistance with sample fabrication and materials characterization. We would like to thank Knut and Alice Wallenberg Foundation,

Swedish Research Council, Research Council of Norway and the Swedish Foundation for Strategic Research for the financial support. We acknowledge the access to HPC resources at USIT/Oslo through NOTUR and at BSC-CNS/ Barcelona through PRACE.

[1]H. Katagiri, K. Jimbo, W. S. Maw, K. Oishi, M. Yamazaki, H. Araki, and A. Takeuchi, Thin Solid Films **517**(7), 2455–2460 (2009).
[2]M. A. Green, K. Emery, Y. Hishikawa, W. Warta, and E. D. Dunlop, Prog. Photovoltaics **24**(1), 3–11 (2016).
[3]K.-J. Yang, D.-H. Son, S.-J. Sung, J.-H. Sim, Y.-I. Kim, S.-N. Park, D.-H. Jeon, J. Kim, D.-K. Hwang, C.-W. Jeon, D. Nam, H. Cheong, J.-K. Kang, and D.-H. Kim, J. Mater. Chem. A **4**, 10151–10158 (2016).
[4]T. Dullweber, G. H. Anna, U. Rau, and H. W. Schock, Sol. Energy Mater. Sol. Cells **67**(1–4), 145–150 (2001).
[5]A. Chirilă, S. Buecheler, F. Pianezzi, P. Bloesch, C. Gretener, A. R. Uhl, C. Fella, L. Kranz, J. Perrenoud, S. Seyrling, R. Verma, S. Nishiwaki, Y. E. Romanyuk, G. Bilger, and A. N. Tiwari, Nat. Mater. **10**(11), 857–861 (2011).
[6]R. Caballero, I. Victorov, R. Serna, J. M. Cano-Torres, C. Maffiotte, E. Garcia-Llamas, J. M. Merino, M. Valakh, I. Bodnar, and M. León, Acta Mater. **79**, 181–187 (2014).
[7]J. Li, H. Du, J. Yarbrough, A. Norman, K. Jones, G. Teeter, F. L. Terry, and D. Levi, Opt. Express **20**(S2), A327–A332 (2012).
[8]S. G. Choi, H. Y. Zhao, C. Persson, C. L. Perkins, A. L. Donohue, B. To, A. G. Norman, J. Li, and I. L. Repins, J. Appl. Phys. **111**(3), 033506 (2012).
[9]S.-Y. Li, C. Hägglund, Y. Ren, J. J. S. Scragg, J. K. Larsen, C. Frisk, K. Rudisch, S. Englund, and C. Platzer-Björkman, Sol. Energy Mater. Sol. Cells **149**, 170–178 (2016).
[10]Ö. Demircioğlu, M. Mousel, A. Redinger, G. Rey, T. Weiss, S. Siebentritt, I. Riedel, and L. Gütay, J. Appl. Phys. **118**(18), 185302 (2015).
[11]S. Levcenko, G. Gurieva, M. Guc, and A. Nateprov, Moldavian J. Phys. Sci. **8**(2), 173–177 (2009).
[12]N. Ross, J. Larsen, S. Grini, E. Särhammar, L. Vines, and C. Platzer-Björkman, in Proceedings of the 43rd IEEE PVSC (2016).
[13]J. K. Larsen, Y. Ren, N. Ross, E. Särhammar, S. Y. Li, and C. Platzer-Björkman, "Surface modification through air annealing $Cu_2ZnSn(S,Se)_4$ absorbers," Thin Solid Films (to be published).
[14]D. E. Aspnes, J. B. Theeten, and F. Hottier, Phys. Rev. B **20**, 3292–3302 (1979).
[15]C. G. Granqvist and O. Hunderi, Phys. Rev. B **16**(8), 3513–3534 (1977).
[16]D. Lehmann, F. Seidel, and D. Zahn, SpringerPlus **3**(1), 82 (2014).
[17]C. Klingshrin, *Semiconductor Physics* (Springer-Verlag, Berlin/Heidelberg, 2005).
[18]G. Kresse and J. Furthmüller, Phys. Rev. B **54**, 11169–11186 (1996).
[19]J. Heyd, G. E. Scuseria, and M. Ernzerhof, J. Chem. Phys. **118**(18), 8207–8215 (2003).
[20]A. D. Becke and E. R. Johnson, J. Chem. Phys. **124**(22), 221101 (2006).
[21]W. Setyawan, R. Gaume, S. Lam, R. S. Feigelson, and S. Curtarolo, ACS Comb. Sci. **13**, 382–390 (2011).
[22]J. P. Perdew, A. Ruzsinszky, G. a. I. Csonka, O. A. Vydrov, G. E. Scuseria, L. A. Constantin, X. Zhou, and K. Burke, Phys. Rev. Lett. **100**, 136406 (2008).
[23]S. Zamulko, R. Chen, and C. Persson, "First-principles analysis of $Cu_2Zn(Sn,Si/Ge)(S/Se)_4$ alloys for solar cell applications," Phys. Status Solidi C (submitted).
[24]P. Lautenschlager, M. Garriga, S. Logothetidis, and M. Cardona, Phys. Rev. B **35**, 9174–9189 (1987).
[25]R. W. A. F. Collins and S. Andre, in *Handbook of Ellipsometry*, edited by H. G. A. I. Tompkins and A. Eugene (William Andrew, Inc. and Springer-Verlag GmbH & Co. KG, 2005), pp. 153.
[26]S. G. Choi, T. J. Kim, S. Y. Hwang, J. Li, C. Persson, Y. D. Kim, S. H. Wei, and I. L. Repins, Sol. Energy Mater. Sol. Cells **130**, 375–379 (2014).
[27]E. Garcia-Llamas, J. M. Merino, R. Serna, X. Fontané, I. A. Victorov, A. Pérez-Rodríguez, M. León, I. V. Bodnar, V. Izquierdo-Roca, and R. Caballero, Sol. Energy Mater. Sol. Cells **158**, 147–153 (2016).
[28]C. Persson, J. Appl. Phys. **107**(5), 053710 (2010).
[29]C. Persson, R. Chen, H. Zhao, M. Kumar, and D. Huang, *Copper Zinc Tin Sulfide-Based Thin-Film Solar Cells* (John Wiley & Sons Ltd., 2014), pp. 75–105.
[30]M. Kumar, H. Zhao, and C. Persson, Thin Solid Films **535**, 318–321 (2013).
[31]J. Li, J. Chen, and R. W. Collins, Appl. Phys. Lett. **97**(18), 181909 (2010).
[32]O. Madelung, *Semiconductor - Basic Data*, 2nd ed. (Springer, Berlin, 1996).
[33]N. M. Ravindra, P. Ganapathy, and J. Choi, Infrared Phys. Technol. **50**(1), 21–29 (2007).
[34]W. Q. Hong, J. Phys. D: Appl. Phys. **22**(9), 1384 (1989).
[35]B. D. Viezbicke, S. Patel, B. E. Davis, and D. P. Birnie, Phys. Status Solidi B **252**(8), 1700–1710 (2015).
[36]J. He, L. Sun, S. Chen, Y. Chen, P. Yang, and J. Chu, J. Alloys Compd. **511**(1), 129–132 (2012).
[37]S. Chen, A. Walsh, J.-H. Yang, X. G. Gong, L. Sun, P.-X. Yang, J.-H. Chu, and S.-H. Wei, Phys. Rev. B **83**, 125201 (2011).